Available online at www.sciencedirect.com
ScienceDirect
Trans. Nonferrous Met. Soc. China 30(2020) 1771−1779
Transactions of Nonferrous Metals Society of China
www.tnmsc.cn

High temperature mechanical properties and microstructure of die forged Al−5.87Zn−2.07Mg−2.42Cu alloy

Yao LI[1], Guo-fu XU[1,2], Xiao-yan PENG[1], Shi-chao LIU[1], Yu-hai DOU[3], Xiao-peng LIANG[1]

1. School of Materials Science and Engineering, Central South University, Changsha 410083, China;
2. Key Laboratory of Nonferrous Materials Science and Engineering, Ministry of Education, Changsha 410083, China;
3. Centre for Clean Environment and Energy, Griffith University, Gold Coast, QLD 4222, Australia

Received 27 June 2019; accepted 18 June 2020

Abstract: The high temperature mechanical properties (250 °C) and microstructure of a die-forged Al−5.87Zn−2.07Mg−2.42Cu alloy after T6 heat treatment were investigated. High temperature tensile tests show that as the temperature increases from room temperature to 250 °C, the ultimate tensile strength of the alloy decreases from 638 to 304 MPa, and the elongation rises from 13.6% to 20.4%. Transmission electron microscopy (TEM) and electron backscattered diffraction (EBSD) were applied for microstructure characterization, which indicates that the increase of tensile temperature can lead to the coarsening of precipitates, drop of dislocation density, and increase of dynamic recovery. After tensile testing at 250 °C, a sub-grain structure composed of a high fraction of small-angle grain boundary is formed.

Key words: Al−Zn−Mg−Cu alloy; dynamic recovery; high temperature mechanical properties; microstructure

1 Introduction

Al−Zn−Mg−Cu alloys possess the advantages of high specific strength, high specific stiffness and good processing performance, and have been widely used for various applications such as aircraft components, high-stress structural parts and aerospace structural components [1−3]. During the service Al−Zn−Mg−Cu alloys often meet the challenge from high temperature conditions, during which their flow behavior is complicated [4,5]. Different mechanical and microstructure responses, such as work hardening [6,7], dynamic recovery [8] and dynamic recrystallization [9−11], often occur during deforming at high temperatures and influence their mechanical performance [12,13]. In addition, dynamic precipitation and precipitates coarsening normally occur during high temperature deformation [14]. To date, researchers have done tremendous research on the strengthening mechanisms of Al alloys and the influence of heat treatment on the microstructure and mechanical properties of 7 series aluminum alloy. CHEN et al [15] studied the effect of homogenization on the microstructure and properties of extruded Al−Zn−Mg alloy. It was found that during the homogenization process, the eutectic phase was dissolved or transformed into *S* phase, and iron-rich phase can be partially dissolved. In addition, CHEN et al [16] also studied the evolution of grain structure, microstructure and second phase of Al−Zn−Mg alloy during extrusion. They found that in the weld zone, the alloy underwent dynamic recrystallization and evenly distributed $MgZn_2$ and coarse $Al_{23}CuFe_4$ phase were also observed in the

Foundation item: Project (220636) supported by the Postdoctoral Science Foundation of the Central South University, China; Project (2016B090931004) supported by the Guangdong Province Science and Research Plan, China; Project (51601229) supported by the National Natural Science Foundation of China
Corresponding author: Xiao-peng LIANG; Tel: +86-18684894344; E-mail: liangxp@csu.edu.cn
DOI: 10.1016/S1003-6326(20)65337-7

alloy. XU et al [17] studied the effects of solid solution, severe deformation and ageing on the mechanical properties of 7085 aluminum alloy. It was found that the tensile strength of 7085 aluminum alloy was increased by 187 MPa due to the dislocation strengthening effect caused by extrusion. YANG et al [18] studied the softening mechanisms of 7085 aluminum alloy under isothermal compression with different rates. It was found that dynamic recovery can provide high stored energy for discontinuous dynamic recrystallization, resulting in the retardation in the occurrence of continuous dynamic recrystallization. ROVEN et al [14] studied the precipitation behavior of the Al−Mg−Si alloy during equal-channel angular pressing at room temperature and 175 °C. Dynamic precipitation was observed during severe plastic deformation at both temperatures and reasons for dynamic precipitation were analyzed and compared with those in conventional static aging. Besides, many studies also focused on the high temperature properties of aluminum alloys. However, most of them focused on the high temperature super-plasticity, and the changes in strength of alloys at medium and high temperatures were scarcely reported. KUMAR et al [19] studied the superplastic behavior of Al−Zn−Mg−Cu−Zr alloy containing Sc. They found that when the alloy is stretched at 475 °C, the elongation can reach 650%.

Al−Zn−Mg−Cu alloys, as a forged connecting rod, will inevitably be heated up and serve in high temperature working conditions for a long time. In this study, the effects of temperature on the mechanical properties of Al−Zn−Mg−Cu alloys and the softening mechanisms were studied by tensile testing and microstructure characterization.

2 Experimental

The experimental samples were cut from a hot die forged connecting rod, as shown in Fig. 1(a). The composition of studied alloy is Al−5.87Zn−2.07Mg−2.42Cu−0.1Mn−0.10Zr−0.11Fe−0.16Si (in wt.%). The sampling section is shown in Fig. 1(b). These samples were first subjected to a solution treatment at 475 °C for 1.5 h, and then subjected to T6 peak aging treatment (120 °C for 24 h). The schematic illustration of the testing sample is shown in Fig. 1(c). The high temperature tensile tests were performed on an MTS810 tester with MTS 653.02 heating apparatus. The test temperature was set to be room temperature, 100, 150, 200 and 250 °C, respectively. The tensile experiments were conducted at a strain rate of 0.2 mm/min after holding at a specified temperature for 15 min, and for every test condition three parallel tests were carried out.

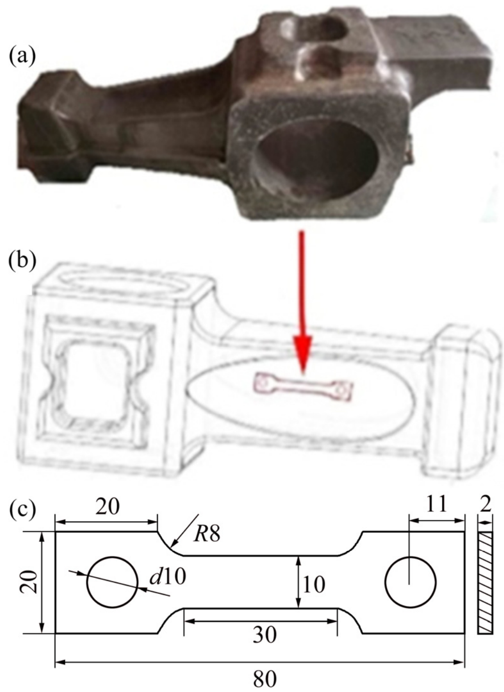

Fig. 1 Alloy sampling diagram: (a) Original part drawing; (b) Sampling position diagram; (c) Tensile bar (unit: mm)

The scanning electron microscopy (SEM) observation was carried out on a Sirion 200 field emission scanning electron microscope, operating at 20 kV. Electron backscattered diffraction (EBSD) data were collected by SEM equipped with XM4 Hikari and analyzed by OIM 5.31 software. The EBSD samples were selected parallel to the tensile direction, and electropolished in 75% methanol and 25% nitric acid mixed solution. G^2F20 transmission electron microscopy (TEM) observation, operating at 200 kV, was used to characterize the evolution of microstructure. The sample for TEM observation was mechanically polished to a thickness of about 80 μm and then electropolished in 75% methanol and 25% nitric acid mixed solution at temperatures between −30 and −20 °C.

3 Results

3.1 Mechanical properties

The ultimate tensile strength (UTS), yield strength (YS) and elongation of the Al−Zn−Mg−Cu alloy obtained under different temperatures are shown in Fig. 2. It is obvious that both the YS and UTS decreased with the increase of testing temperature. And with the increase of temperature, the rate of YS decline significantly increased. The elongation increased with the increase of testing temperature. As the testing temperature increased from room temperature to 250 °C, the UTS decreased from 638 to 304 MPa, the YS decreased from 479 to 251 MPa, and the elongation increased from 13.6% to 20.4%.

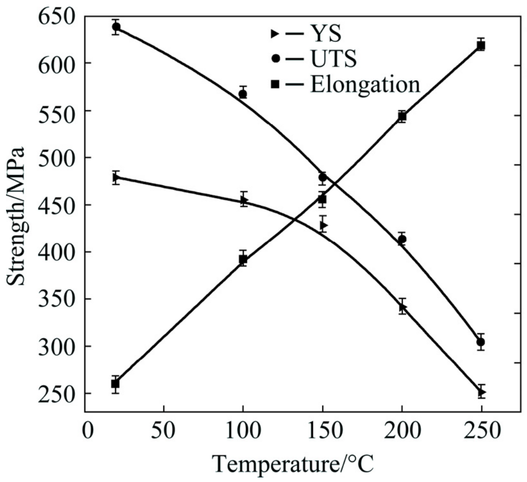

Fig. 2 Mechanical properties of alloy during high temperature tensile deformation

3.2 Fracture morphology

Figure 3 shows SEM images of the fracture morphology of Al−5.87Zn−2.07Mg−2.42Cu alloys after tensile test from room temperature to 250 °C. It can be clearly seen that fracture mode has both transgranular ductile fracture and intergranular brittle fracture. Abundant coarse phases were found in the dimples when the alloy was deformed at room temperature. As the tensile temperature increased to 100 °C, the number of fracture dimples gradually increased, but a few fracture planes could still be seen. In contrast, many equal-sized dimples were also formed when the alloy was deformed at 150 °C, while the dimples were significantly refined (Fig. 3(c)), and the fracture plane was reduced compared to 100 °C. When the alloy was stretched at 200 °C, the fracture morphology changed significantly, the dimple size increased, and the fracture plane disappeared. When the stretching temperature increased to 250 °C, the dimples became large and deep, and sliding steps could be observed.

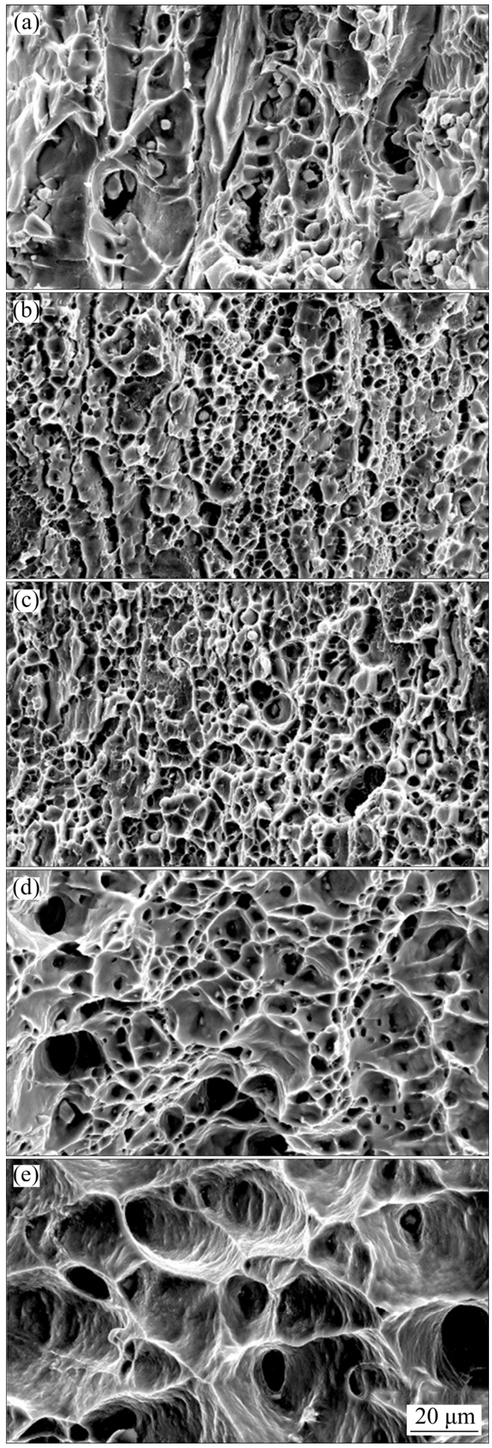

Fig. 3 SEM images of fracture structure after tensile deformation at different temperatures: (a) Room temperature; (b) 100 °C; (c) 150 °C; (d) 200 °C; (e) 250 °C

3.3 Dislocation morphology

Figure 4 shows the TEM images of T6-aged alloys showing dislocation evolution at different temperatures. As can be seen, dislocations were densely distributed in the matrix when the alloys were stretched at room temperature. When temperature rose to 150 °C, the number of dislocations decreased and the distribution became more dispersed. By contrast, the dislocation density was significantly reduced when the temperature increased to 250 °C.

3.4 Precipitates morphology

Figures 5 and 6 show the TEM images of the precipitates and selected area electron diffraction (SAED) patterns taken from [100] zone axis of T6-aged Al−5.87Zn−2.07Mg−2.42Cu alloy after tensile test at different temperatures, respectively. When the alloys were stretched at room temperature, the main precipitates of the alloys were the GP zones and the η' phases which maintained a coherent and semi-coherent relationship with the matrix, as shown in Fig. 5(a) and Fig. 6(a). However, it is worth noting that due to the short stretching time, as the stretching temperature increased to 100 and 150 °C, there was no significant change in the type and size of the precipitates and the type of precipitates was mainly

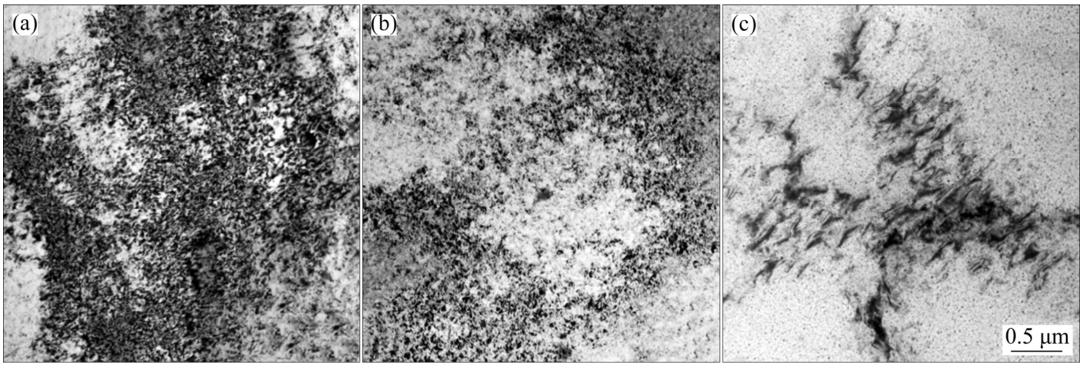

Fig. 4 TEM images of T6-aged alloys showing dislocation evolution at different temperatures: (a) Room temperatures; (b) 150 °C; (c) 250 °C

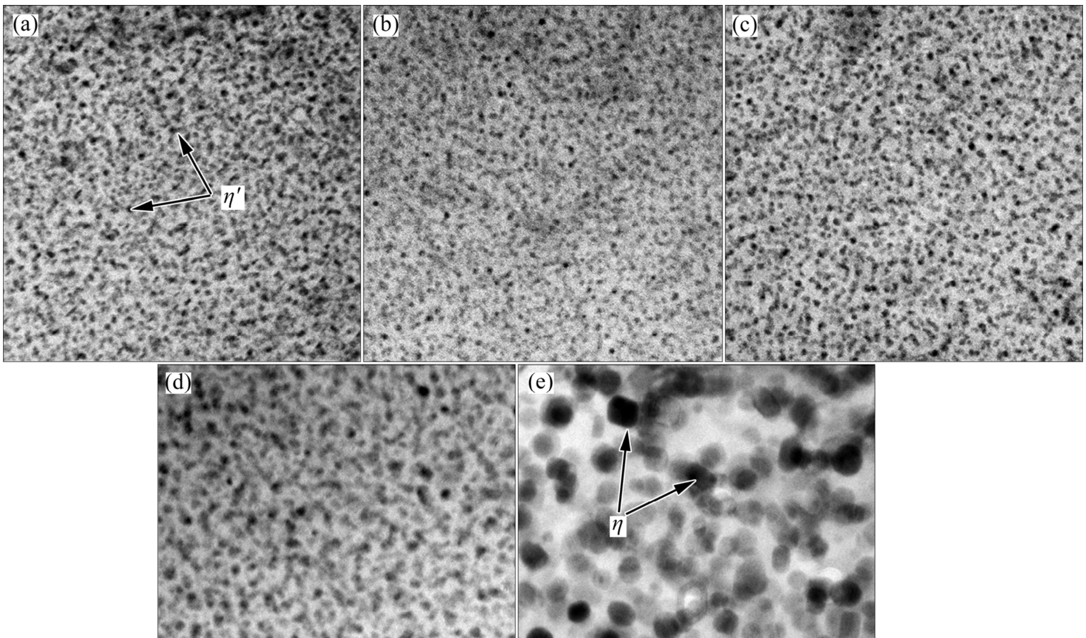

Fig. 5 TEM images of precipitates after tensile test at different temperatures: (a) Room temperature; (b) 100 °C; (c) 150 °C; (d) 200 °C; (e) 250 °C

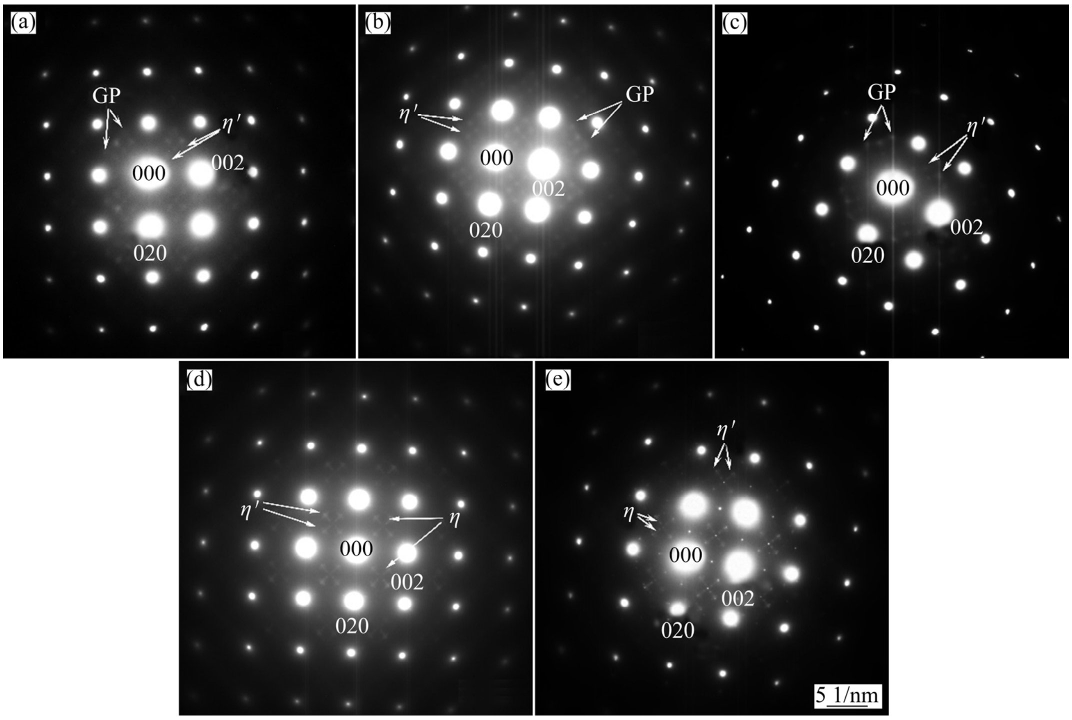

Fig. 6 SAED patterns taken from [100] zone axis of T6-aged alloys after tensile test at different temperatures: (a) Room temperature; (b) 100 °C; (c) 150 °C; (d) 200 °C; (e) 250 °C

dominated by the GP zone and the η' phase. By contrast, when the stretching temperature increased to 200 °C, because the stretching temperature was much higher than the alloy peak aging temperature, precipitates were significantly coarsened, as shown in Fig. 5(d), and the type of precipitates changed to η' and η phases, as shown in Fig. 6(d). Precipitates of the alloys were also significantly coarsened when the stretching temperature rose continuously to 250 °C, and the η phases became the main precipitates which were non-coherent with the matrix.

3.5 Dynamic recovery behavior during high temperature tensile test

The EBSD IPF maps of the alloys stretched at different temperatures are presented in Fig. 7. It can be seen that the grains of the as-forged alloy were almost equiaxed. But grains were obviously elongated along the stretching direction after the tensile test, and the recovery of the alloys occurred to different degrees as the stretching temperature increased, as shown in the black dotted ellipses in Fig. 7. And when the temperature increased to 250 °C, it could be clearly observed that the sub-grain structure was composed of small-angle grain boundaries in the later recovery period. However, due to the low stretching temperature, no obvious recrystallized structure was observed.

4 Discussion

4.1 Precipitate states of alloy during high temperature tensile test

In general, the precipitation order of 7xxx alloys follows the sequence of α-supersaturated solid solution → GP zones → η' → η ($MgZn_2$) [20,21]. The process of precipitation of Al−Zn−Mg−Cu alloys is not independent, and the precipitation and growth of various precipitates influence each other. Therefore, it is possible to promote several complex precipitation processes at the same time during high temperature tensile deformation. For the isothermal precipitation process, the precipitation driving force (Δg) can be described as [22,23]

$$\Delta g = \frac{kT}{v_{\mathrm{at}}}\ln\left(\frac{C}{C_{\mathrm{eq}}}\right) \tag{1}$$

where v_{at} is the atomic volume of precipitates (considered as a constant for all specimens), k is the Boltzmann's constant, T is the thermodynamic

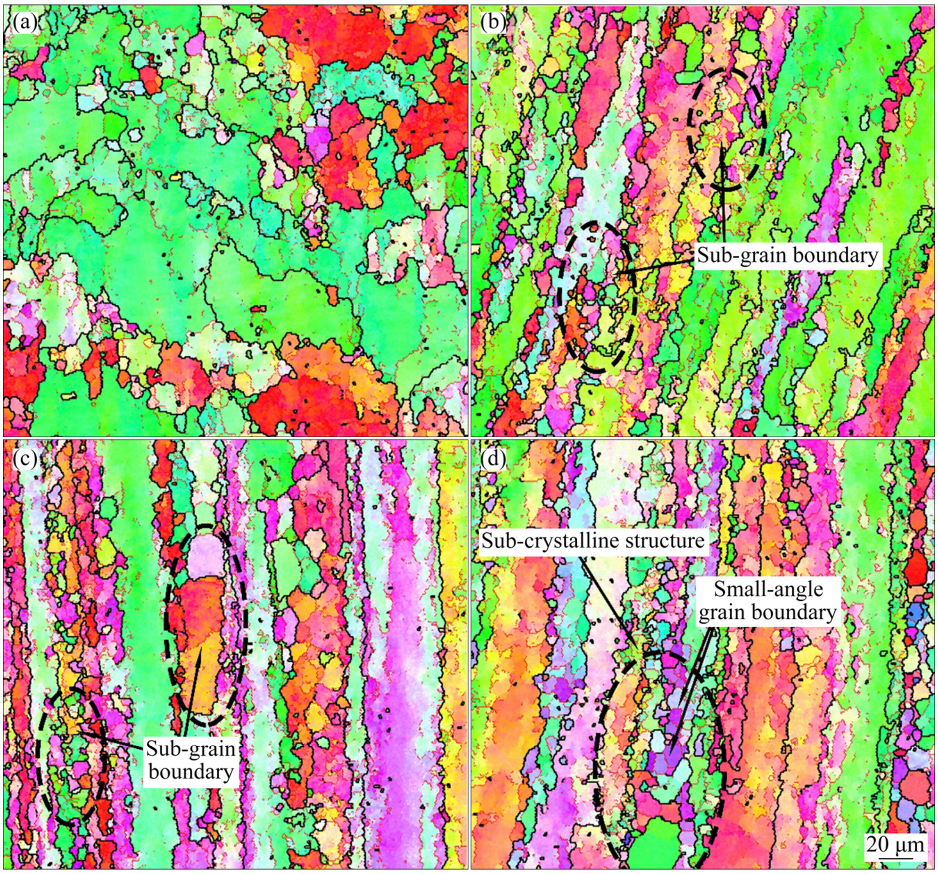

Fig. 7 EBSD IPF maps of die-forged alloys (a) and those after tensile test at different temperatures (b−d): (b) Room temperature; (c) 150 °C; (d) 250 °C

temperature, C_{eq} is the equilibrium solute concentration of the matrix, and C is the current solute concentration of the matrix. It can be seen from Eq. (1) that the driving force for precipitation increases with the increase of the aging temperature. However, the precipitate nuclei will not grow until it reaches the critical nucleation radius. The critical nucleation radius (R*) can be written as [22,23]

$$R^*=\frac{2\gamma v_{at}}{kT\ln(C/C_{eq})} \tag{2}$$

where γ is the interfacial energy between precipitate and matrix. It can be seen from Eq. (2) that as the temperature rises, the critical nucleation radius decreases.

According to the Gibbs−Thomson effect [24], the solute solubility particle in the matrix adjacent to the particle will increase as the radius of the particle or curvature of the surface decreases, so there is a gradient of solubility in the matrix between particles with different sizes. According to the Gibbs−Thomson effect, smaller particles with curvature surface will dissolve faster into a matrix, which leads to the dissolution of small particles and the growth of large particles. This process is called Ostawald coarsening. The following equation describes the Ostwarld coarsening kinetics [25]:

$$\bar{r}^3-r_0^3=D\gamma X_e t \tag{3}$$

where $\bar{r}$ is the average radius of precipitates in the crystal, r_0 is the average radius at time t=0, D is the diffusion coefficient, and X_e is the average solid solubility of larger particles. D and X_e increase exponentially with the increase of the temperature. Therefore, the coarsening of precipitates is accelerated as the temperature increases.

Therefore, the evolution of precipitates during the high temperature tensile process depends on not only the Δg, but also the size distribution of precipitates according to Ostwald coarsening [26]. As shown in Fig. 5, after the T6 aging sample was stretched at room temperature, the size of the precipitates was small and dispersed. When the stretching temperature rose to 150 °C, Δg was significantly increased according to Eq. (1). However, due to the short stretching time and small temperature difference, no obvious differences in morphology were observed between different precipitates. In comparison, when the temperature rose to 250 °C, Δg was significantly increased, and according to the combination theory of Eq. (3), precipitates were coarsened to form η phases, as shown in Fig. 5.

4.2 Dynamic recovery of alloy during high temperature tensile test

The dynamic recovery process of alloys during thermal processing is complex. It occurs under the combined action of external force and temperature. During thermal processing, in the early stage of dynamic recovery, the dislocation density gradually decreases. In the medium stage, as the deformation progresses, the dislocations are congested and appear polygonal. In the later stage of dynamic recovery, many subcrystalline structures will be formed in the alloy. During high temperature stretching, as the amount of deformation increases, dislocation entanglements and cellular substructures begin to form. However, due to the increase in deformation temperature, thermal activation conditions are provided for the recovery process. The dislocation density is continuously reduced by the migration of edge dislocations, the slip of screw dislocations, the unpinning of the dislocation nodes, and the subsequent cancellation of the dislocations on the new slip surface. When the strain rate and the deformation temperature increase, the dislocation forming rate is lower than the dislocation cancellation rate, the strength of the alloys decreases, representing a dynamic recovery effect. In addition, as the dynamic recovery progresses, in the later stage of the dynamic recovery, a sub-grain structure composed of small-angle grain boundaries will appear. However, due to the influence of high temperature and other factors, the subcrystalline structure formed by dynamic recovery cannot continue to grow into recrystallized grains.

As shown in Fig. 2, as the deformation temperature increases, the alloy elongation gradually increases. When the alloy is stretched at room temperature, the low deformation temperature leads to lower thermal activation energy and dislocation thermal movement rate. Thus, dislocation annihilation occurs less obviously during the rapid aggregation process. At this time, dislocations appear agglomerated and block each other's movement (Fig. 4(a)), thus effectively strengthening the alloy. However, as the temperature increases, the thermal activation energy of the alloy increases gradually, and the dislocation motion increases. When the shaped dislocations meet, the offset will occur and many deformed structures will be formed in the grains (Fig. 7). At this time, the density of dislocations decreases and the obstacle effect between each other decreases with the increase of temperature, as shown in Figs. 4(b) and (c). In addition, as the temperature increases, the precipitates are also coarsened. So as shown in Fig. 2, the YS of alloy drops sharply after 150 °C.

4.3 Effect of microstructure on mechanical properties

The main strengthening mechanisms of the 7xxx aluminum alloys are precipitation strengthening and dislocation strengthening. The interaction between the precipitates and dislocations results in a significant improvement in alloy properties [27]. The typical shearing mechanism and the Orowan bypass mechanism can explain the improvement brought by precipitates. The shearing mechanism is a strengthening response in which the precipitates are sheared by the dislocation and the Orowan strengthening is a strengthening mechanism describing dislocations bypass the particles [28]. For Al−Zn−Mg−Cu alloys, when the precipitates are fine η' phases or GP regions that maintain a coherent relationship with the matrix, the movement of dislocations can be effectively hindered. At this time, the dislocations have to cut through the precipitates and thus contribute to the yield strength $\Delta\sigma_A$, which can be expressed as [29]

$$\Delta\sigma_A=c_1 f^m r^n \tag{4}$$

where c_1, m and n are constants, and f and r are the volume fraction and radius of precipitates, respectively.

During the thermal deformation process, the precipitates undergo significant coarsening at high temperature, forming η phases which are not coherent with the matrix. At this point, dislocations should only bypass the precipitates during the deformation. The yield strength $\Delta\sigma_B$ can be expressed as

$$\Delta\sigma_B=c_2 f^{1/2} r^{-1} \tag{5}$$

where c_2 is a constant. It can be seen from Eq. (5) that as the radius of the precipitates increases, the yield strength decreases.

Therefore, the size and type of precipitates play a crucial role in the properties of alloys. When precipitates are small, dislocations may cut through these particles. As a result, precipitates and dislocation density increase, and strengths of the alloy are improved. When precipitates are coarsened during deformation at high temperatures, the dislocations cannot cut through secondary phases due to their large size and the bypass model may work, resulting in the degradation of the strengths. When T6 alloys are deformed at room temperature, the precipitates are mainly fine η' phases and the GP zones, as shown in Figs. 5(a) and (b). Hence, dislocations may cut through the particles, and the UTS can reach 638 MPa. However, as the stretching temperature rises to 150 °C, although there is no significant change in the size and coherence of precipitates, alloys undergo dynamic recovery and the dislocation density significantly reduces, as shown in Fig. 4(b). When the deformation temperature is increased to 250 °C, precipitates are apparently coarsened to form the η phases, as shown in Fig. 5(e). At this time, dislocations can only bypass second phases. As shown in Eq. (5), as the size of the precipitates increases gradually, the strengths gradually decrease. In addition, when samples are stretched at 250 °C, a part of deformation dislocation structure is consumed and many sub-crystalline structures composed of small-angle grain boundary structures are formed, the strength is reduced to 304 MPa, and the rate of strength decrease is significantly increased, as shown in Fig. 2.

5 Conclusions

(1) When the high temperature stretching temperature is increased from room temperature to 250 °C, the tensile strength of the Al−5.87Zn−2.07Mg−2.42Cu alloy is reduced from 638 to 304 MPa, and the elongation increases from 13.6% to 20.4%.

(2) When the stretching temperature is raised to 150 °C, the precipitates do not change significantly, and the η' phase and the GP zone are still dominant. When the stretching temperature is raised to 250 °C, the precipitates are coarsened to form the η phase.

(3) When the alloy is stretched at a speed of 0.2 mm/min, the alloy undergoes dynamic recovery and the dislocation density decreases. Many sub-crystalline structures composed of small-angle grain boundary structures are formed as the stretching temperature increases.

References

[1] DURSUN T, SOUTIS C. Recent developments in advanced aircraft aluminium alloys [J]. Materials & Design, 2014, 56(4): 862−871.

[2] WEN Kai, FAN Yun-qiang, WANG Guo-jun, JIN Long-bin, LI Xi-wu, LI Zhi-hui, ZHANG Yong-an. Aging behavior and precipitate characterization of a high Zn-containing Al−Zn−Mg−Cu alloy with various tempers [J]. Materials & Design, 2016, 101(1): 16−23.

[3] WANG S S, JIANG J T, FAN G H, PANINDRE A M, FRANKEL G S, ZHEN L. Accelerated precipitation and growth of phases in an Al−Zn−Mg−Cu alloy processed by surface abrasion [J]. Acta Materialia, 2017, 131: 233−245.

[4] LIN Y C, CHEN X M. A critical review of experimental results and constitutive descriptions for metals and alloys in hot working [J]. Materials & Design, 2011, 32(4): 1733−1759.

[5] SALEHI M S, SERAJZADEH S. Simulation of static recrystallization in non-isothermal annealing using a coupled cellular automata and finite element model [J]. Computational Materials Science, 2012, 53(1): 145−152.

[6] HE Yun-bin, PAN Qing-lin, CHEN Qin, ZHANG Zhi-ye, LIU Xiao-yan. Modeling of strain hardening and dynamic recrystallization of ZK60 magnesium alloy during hot deformation [J]. Transactions of the Nonferrous Metals Society of China, 2012, 22(2): 246−254.

[7] PUCHI-CABRERA E S, STAIA M H, GUERIN J D, LESAGE J, DUBAR M, CHICOT D. Analysis of the work-hardening behavior of C−Mn steels deformed under hot-working conditions [J]. International Journal of Plasticity, 2013, 51(6): 145−160.

[8] LIN Y C, CHEN X M, WEN D X, CHEN M S. A physically-based constitutive model for a typical nickel-based superalloy [J]. Computational Materials Science, 2014, 83: 282−289.

[9] LIN Y C, CHEN M S, ZHONG J. Study of static recrystallization kinetics in a low alloy steel [J]. Computational Materials Science, 2009, 44(2): 316−321.

[10] LIN Y C, CHEN M S, ZHONG J. Study of metadynamic recrystallization behaviors in a low alloy steel [J]. Journal of Materials Processing Technology, 2009, 209(5): 2477−2482.

[11] LIU Y G, LIU J, LI M Q, LIN H. The study on kinetics of static recrystallization in the two-stage isothermal compression of 300M steel [J]. Computational Materials Science, 2014, 84(1): 115−121.

[12] HAGHDADI N, ZAREI-HANZAKI A, ABEDI H R, SABOKPA O. The effect of thermomechanical parameters on the eutectic silicon characteristics in a non-modified cast A356 aluminum alloy [J]. Materials Science and Engineering A, 2012, 549(7): 93−99.

[13] SAMANTARAY D, MANDAL S, KUMAR V, ALBERT S K, BHADURI A K, JAYAKUMAR T. Optimization of processing parameters based on high temperature flow behavior and microstructural evolution of a nitrogen enhanced 316L(N) stainless steel [J]. Materials Science and Engineering A , 2012, 552(1): 236−244.

[14] ROVEN H J, LIU M, WERENSKIOLD J C. Dynamic precipitation during severe plastic deformation of an Al−Mg−Si aluminium alloy [J]. Materials Science and Engineering A, 2008, 483(8): 54−58.

[15] CHEN Liang, YUAN Sheng-wei, LI Zhi-gang, ZHENG Wei, ZHAO Guo-qun, ZHANG Cun-sheng. Influence of homogenization treatment on microstructure and mechanical properties of Al−Zn−Mg alloy extruded by porthole die [J]. Materials Characterization, 2020, 161: 110148.

[16] CHEN Liang, CHEN Gao-jin, TANG Jian-wei, ZHAO Guo-qun, ZHANG Cun-sheng. Evolution of grain structure, micro-texture and second phase during porthole die extrusion of Al−Zn−Mg alloy [J]. Materials Characterization, 2019, 158: 109953.

[17] XU Xiao-jing, WANG Zi-lu, LU Wen-jun, GUO Yun-fei, MA Wen-hai, CHEN Yang, XU Chi. Strengthening mechanisms of 7085 aluminum alloy by solution-large deformation-aging [J]. Rare Metal Materials and Engineering, 2017, 46(4): 1008−1012.

[18] YANG Q Y, DENG Z H, ZHANG Z Q, LIU Q, JIA Z H, HUANG G J. Effects of strain rate on flow stress behavior and dynamic recrystallization mechanism of Al−Zn−Mg−Cu aluminum alloy during hot deformation [J]. Materials Science and Engineering A, 2016, 662: 204−213.

[19] KUMAR A, MUKHOPADHYAY A K, PRASAD K S. Superplastic behaviour of Al−Zn−Mg−Cu−Zr alloy AA7010 containing Sc [J]. Materials Science and Engineering A, 527(3): 854−857.

[20] BERG L K, GJONNES J, HANSEN V, LI X Z, KNUTSON-WEDEL G, WATERLOO G, SCHRYVERS D, WALLENBERG L R. GP-zones in Al−Zn−Mg alloys and their role in artificial aging [J]. Acta Materialia, 2001, 49(17): 3443−3451.

[21] HADJADJ L, AMRIA R, HAMANA D, MOSBAH A. Characterization of precipitation and phase transformations in Al−Zn−Mg alloy by the differential dilatometry [J]. Journal of Alloys and Compounds, 2008, 462(1): 279−283.

[22] AARONSON H I, KINSMAN K R, RUSSELL K C. The volume free energy change associated with precipitate nucleation [J]. Scripta Metallurgica, 1970, 4(2): 101−106.

[23] DESCHAMPS A, BRECHET Y, Influence of predeformation and ageing of an Al−Zn−Mg alloy (II). Modeling of precipitation kinetics and yield stress [J]. Acta Materialia, 1998, 47(1): 293−305.

[24] MCLEAN J G, KRISHNAMACHARI B, PEALE D R, CHASON E, SETHNA J P, COOPER B H. Decay of isolated surface features driven by the Gibbs−Thomson effect in analytic model and simulation [J]. Oalib Journal, 1996, 55(3): 1811−1823.

[25] WEN Y H, WANG Y, CHEN L Q. Coarsening dynamics of self-accommodating coherent patterns [J]. Acta Materialia, 2002, 50(1): 13−21.

[26] PENG Xiao-yan, LI Yao, LIANG Xiao-peng, GUO Qi, XU Guo-fu, DENG Ying, YIN Zhi-min. Precipitate behavior and mechanical properties of enhanced solution treated Al−Zn−Mg−Cu alloy during non-isothermal ageing [J]. Journal of Alloys and Compounds, 2018, 735: 964−974.

[27] FRAGOMENI J M, HILLBERRY B M. A micromechanical method for predicting the precipitation hardening response of particle strengthened alloys hardened by ordered precipitates [J]. Acta Mechanica, 1999, 138(3): 185−210.

[28] KAKA M A, WEN H, HU T, TOPPING T D, SEIDMAN D N, LAVERNIA E J, SCHOENUNG J M. Mechanical behavior and strengthening mechanisms in ultrafine grain precipitation-strengthened aluminum alloy [J]. Acta Materialia, 2014, 62(5): 141−155.

[29] LIU Y, JIANG D M, LI B Q, YANG W S, HU J. Effect of cooling aging on microstructure and mechanical properties of an Al−Zn−Mg−Cu alloy [J]. Materials & Design, 2014, 57(5): 79−86.

模锻态 Al−5.87Zn−2.07Mg−2.42Cu 合金的高温力学性能和显微组织

李 耀[1]，徐国富[1,2]，彭小燕[1]，刘时超[1]，窦玉海[3]，梁霄鹏[1]

1. 中南大学 材料科学与工程学院，长沙 410083；

2. 有色金属科学与工程教育部重点实验室，长沙 410083；

3. Centre for Clean Environment and Energy, Griffith University, Gold Coast, QLD 4222, Australia

摘 要：研究经 T6 时效热处理的模锻态 Al−5.87Zn−2.07Mg−2.42Cu 合金从室温升高到 250 °C 时的高温力学性能和显微组织。高温拉伸试验结果表明，随着拉伸温度从室温升高到 250 °C，合金的抗拉强度从 638 降至 304 MPa，伸长率从 13.6%升至 20.4%。通过透射电子显微镜和电子背散射衍射技术对合金的显微组织进行表征。研究发现，随着拉伸温度的升高，析出相发生粗化，位错密度逐渐降低，合金组织发生不同程度的动态回复。在 250 °C 进行拉伸时，合金内形成许多由小角度晶界组成的亚晶组织。

关键词：Al−Zn−Mg−Cu 合金；动态回复；高温力学性能；显微组织

(Edited by Wei-ping CHEN)